Automatic Quantitative Analysis of Pulmonary Vessels in CT: Methods and Applications

Zhai, Z.

4

Pulmonary vascular morphology associated with gas exchange in systemic sclerosis without lung fibrosis

This chapter was adapted from:

Z. Zhai, M. Staring, M. K. Ninaber, J. K. de Vries-Bouwstra, A. A. Schouffoer, L. J. Kroft, J. Stolk, and B. C. Stoel. **Pulmonary Vascular Morphology Associated With Gas Exchange in Systemic Sclerosis Without Lung Fibrosis**, *Journal of Thoracic Imaging*, Page 373-379, Volume 34(6), 2019 November.

Abstract

Purpose Gas exchange in systemic sclerosis (SSc) is known to be affected by fibrotic changes in the pulmonary parenchyma. However, SSc patients without detectable fibrosis can still have impaired gas transfer. We aim to investigate whether pulmonary vascular changes could partly explain a reduction in gas transfer of systemic sclerosis (SSc) patients without fibrosis.

Materials and Methods We selected 77 patients, whose visual CT scoring showed no fibrosis. Pulmonary vessels were detected automatically in CT images and their local radii were calculated. The frequency of occurrence for each radius was calculated, and from this radius histogram two imaging biomarkers (α and β) were extracted, where α reflects the relative contribution of small vessels compared to large vessels and β represents the vessel tree capacity. Correlations between imaging biomarkers and gas transfer (DLCOc %predicted) were evaluated with Spearman's correlation. Multivariable stepwise linear regression was performed with DLCOc %predicted as dependent variable and age, BMI, sPAP, FEV1 %predicted, TLC %predicted, FVC %predicted, α, β, voxel size and CT-derived lung volume as independent variables.

Results Both α and β were significantly correlated with gas transfer (R=-0.29, p-value=0.011 and R=0.32, p-value=0.004, respectively). The multivariable step-wise linear regression analysis selected sPAP (coefficient=-0.78, 95%CI=[-1.07, -0.49], p-value<0.001), β (coefficient=8.6, 95%CI=[4.07, 13.1], p-value<0.001) and FEV1 %predicted (coefficient=0.3, 95%CI=[0.12, 0.48], p-value=0.001) as significant independent predictors of DLCOc %predicted (R=0.71, p-value<0.001).

Conclusions In SSc patients without detectable pulmonary fibrosis, impaired gas exchange is associated with alterations in pulmonary vascular morphology.

4.1 Introduction

Systemic sclerosis (SSc) is an autoimmune connective tissue disease that involves multiple organs [9]. Pulmonary disease in SSc mainly consists of interstitial lung disease (ILD) and pulmonary hypertension (PH) [10]. For evaluating severity of disease and response to treatment, pulmonary function tests (PFTs), such as diffusion capacity for carbon monoxide (DLCO) and forced vital capacity (FVC), are key outcome measures which play an important role as a surrogate for ILD and PH-related mortality [100]. In SSc-related ILD, structural changes of lung parenchyma, i.e. fibrosis, is known to affect PFTs [10, 101, 102, 103, 104]. In SSc-related PH, DLCO decreases years before diagnosis of PH [13]. Conversely, gas transfer can be mildly or moderately impaired in the absence of detectable pulmonary fibrosis and pulmonary hypertension. Since gas transfer studies measure the alveolar capillary membrane gas exchange efficiency [105], we hypothesized that pulmonary vascular changes might partly explain this impaired DLCO, in the absence of pulmonary fibrosis.

Chest CT is considered the most accurate non-invasive imaging method for pulmonary disease assessment [106]. Some studies on quantifying vascular tree morphology based on CT show promising performances for assessing pulmonary vascular disease [12, 60, 62, 66, 63, 58]. Understanding the relation between vascular structure and pulmonary function may provide specific measurements for evaluating the response to treatment or measuring the severity of pulmonary vascular disease. The aim of this study was to test whether vascular changes were related to impaired gas transfer in SSc patients without fibrosis. To this end, we developed an objective and automatic method to quantify the pulmonary vascular morphology and studied the association between these CT-derived imaging biomarkers and pulmonary function.

4.2 Materials and Methods

4.2.1 Patients

We studied a cohort of 333 consecutive patients who had participated in our annual care program, between April 2009 and October 2015 [92]. The local Medical Ethical Committee approved the protocol and all patients gave written informed consent for collection of clinical and diagnostic data contributing to the biobank of the Leiden Combined Care in SSc (CISS) cohort. From this cohort, 83 patients had a chest CT scan where visual CT scoring showed no fibrosis and had PFTs measured within 8 days of the CT scan. Among these patients, image quality was insufficient for six patients to perform an accurate vascular analysis. Thus, 77 patients were selected for this study. Based on the degree of skin involvement, three subtypes of patients were classified: diffuse cutaneous SSc (DcSSc) with skin involvement proximal to the elbows and knees; limited cutaneous SSc (LcSSc) with skin involvement distal to the elbows and

knees; limited non-cutaneous SSc (LSSc) without skin involvement [107]. The group consisted of 43 never-smokers, 31 ex-smokers and three current smokers.

PFTs were performed under ERS/ATS guidelines [94, 93], including total lung capacity (TLC), forced vital capacity (FVC), forced expiratory volume in 1 second (FEV1) and single-breath diffusion capacity for carbon monoxide corrected for haemoglobin concentration (DLCOc). PFT results were expressed as a percentage of the predicted value (%predicted) [94, 93]. The DLCOc percentage of predicted (DLCOc %predicted) was selected as key outcome measure of gas transfer.

The systolic pulmonary artery pressure (sPAP) was estimated using echocardiography with a commercially available system (Vingmed Vivd7, General Electric Vingmed Ultrasound, Milwaukee, WI, USA). The sPAP was calculated from the tricuspid regurgitation peak gradient and the addition of right atrial pressure [108]. Patients with suspected pulmonary hypertension (PH, echocardiographic sPAP>40 mmHg) were tested by right heart-catheterization (RHC). If the mean pulmonary artery pressure (mPAP) was > 25 mmHg, the individual was diagnosed with PH [109, 110]. Furthermore, the mPAP, cardiac output (CO), pulmonary vascular resistance (PVR) and pulmonary artery wedge pressure (PAWP) were collected and used for determining the type of PH, under the 2015 ESC/ERS guidelines [29]. All patients were scanned with the same CT scanner (Aquilion 64, Toshiba Medical Systems, Otawara, Japan), with full inspiration and without contrast enhancement. The CT settings were: tube voltage = 120kV; tube current=140mA without modulation; rotation time = 0.4s; collimation = 64Ö0.5mm; helical beam pitch = 0.8; images were reconstructed with 0.5 mm slices [25]. Two observers (L.K. and A.S.), who were blinded to the patients' clinical information, scored the CT scans in consensus [11], at five levels: 1) origin of the aortic arch branches; 2) main carina; 3) pulmonary venous confluence; 4) halfway between the third and fifth section; 5) immediately above the right hemi-diaphragm. At each level, six variables were scored as percentages: total disease extent; proportion of ground-glass; extent of reticular pattern; coarseness of reticular disease; extent of emphysema; and presence of bronchiectasis. Patients with 0 percent in all 30 variables were considered to have no parenchymal abnormalities. Patients involved in this study were without any suspicion of pulmonary veno-occlusive disease (PVOD), as the CT scans did not show any signs of ground glass opacities, septal thickening or lymphadenopathy.

4.2.2 CT analysis

For lung segmentation, we employed multi-atlas based methods to flexibly capture anatomical variations, using Elastix registration toolbox [95]. Details on the atlas-based segmentation method can be found in the online supplements. The final segmentation included both left and right lungs. Within each lung, the vascular

Table 4.1: Patient group characteristics

Number of subjects	77
Female n [%]	67 [87]
Age (year)	49.9 ± 14.2
BMI (kg/m^2)	24.6 ± 5.24
sPAP (mmHg) <n=77>	26.9 ± 10.4
mPAP (mmHg) <n=3>	40.3 ±11
CO (L/min) <n=3>	5.17 ± 0.9
PVR ($dyn{\cdot}s/cm^5$) <n=3>	405.3 ± 149
PAWP (mmHg) <n=3>	11 ± 2.6
MRSS	3.38 ± 4.28
Type of SSc n [%]	
DcSSc	8 [10.4]
LcSSc	51 [66.2]
LSSc	18 [23.4]
Autoantibodies, n [%]	
ANA	74 [96.1]
Anti-Scl-70 #	4 [4.2]
Anticentromere *	53 [68.8]
RNA polymerase III	1 [1.3]
Pulmonary function (% predicted**)**	
DLCOc	70.4 ± 16.7
FVC	107 ± 17.4
FEV_1	98.9 ± 16.8
TLC	95.7 ± 12.2
CT-derived measurements	
α	-1.44 ± 0.2
β	10.1 ± 0.62
Lung Volume (L)	4.73 ± 1.24

1 patient with doubtful Anti-Scl-70; * 1 patient with missing data; sPAP, systolic pulmonary arterial pressure, obtained from echocardiography; DcSSc, diffuse cutaneous SSc; LcSSC, limited cutaneous SSc; LSSC, limited non-cutaneous SSc; ANA, antinuclear antibody; Anti-Scl-70, nti-topoisomerase; DLCOc, single-breath diffusion capacity for carbon monoxide corrected with the haemoglobin concentration; FVC, forced vital capacity; FEV_1, forced expiratory volume in 1 second; TLC, total lung capacity.

trees were detected by a graph-cuts method [83], where 'vesselness' and CT intensity were combined into a single cost function. Previously, we evaluated this graph-cuts method using the public data-set from VESSEL12 [69] and obtained accurate vessel segmentation results [111]. 3D views of extracted pulmonary vascular trees are shown in Figure 4.1 (a-c). The entire vascular tree, i.e. both arteries and veins, was automatically extracted and subsequently analysed. In this automatic analysis, the distribution of the different radii of the entire vascular tree was quantified by first calculating the radius within each vessel, then construct a histogram from these data and finally analyse the shape of this histogram, as detailed below.

At each location in the vascular tree, the radius was calculated by a skeletonization method (DtSkeletonization method of Mevislab 2.7 [53]). This method selects voxels that are located at the centre of a blood vessel by eroding the extracted vessels, and the corresponding radius is estimated by measuring the distance between the vessel boundary and the centre. Examples of 'skeletonized' vascular trees are shown in Figure 4.1 (d-f). Subsequently, the number of voxels in the vascular skeleton with a specific radius were counted, producing a histogram of the measured vascular radii. A logarithmic transformation was applied to the frequency of occurrence in order to obtain a linear relation between frequency and radius [112] (Figure 4.1 (g-i)). Thus, the index of each histogram bin represents the vessel radius and the height of the bin represents the logarithm of the number of voxels with that specific radius. We used robust linear regression (robustfit method of MATLAB R2016b [87]) to analyse each radius histogram, and obtained two biomarkers (α, β) corresponding to the slope and intercept of the linear regression, respectively. The slope parameter α reflects the relative contribution of small vessels compared to large vessels (quantifying pruning of small vessels and dilatation of larger vessels) and the intercept β is related to the number of pulmonary capillaries estimated by extrapolation to radius 0, which reflects the vascular tree's capacity. To normalize for inspiration level and lung size, CT-derived lung volume was measured from the lung segmentations. As the vessel radius calculation might be affected by voxel size, the voxel size was also recorded for each patient.

4.2.3 Statistical analysis

For patient characteristics, continuous variables were expressed as means with standard deviations (SD) unless stated otherwise, and categorical variables were expressed as frequencies and percentages. Correlation between DLCOc %predicted or FVC %predicted and age, BMI, sPAP, α, β, CT-derived lung volume were expressed in terms of Spearman's rho correlation. Multivariable linear regression was used to determine independent predictors of DLCOc %predicted. DLCOc %predicted was entered as a dependent variable; age, BMI, sPAP, FEV1 %predicted, TLC %predicted, FVC %

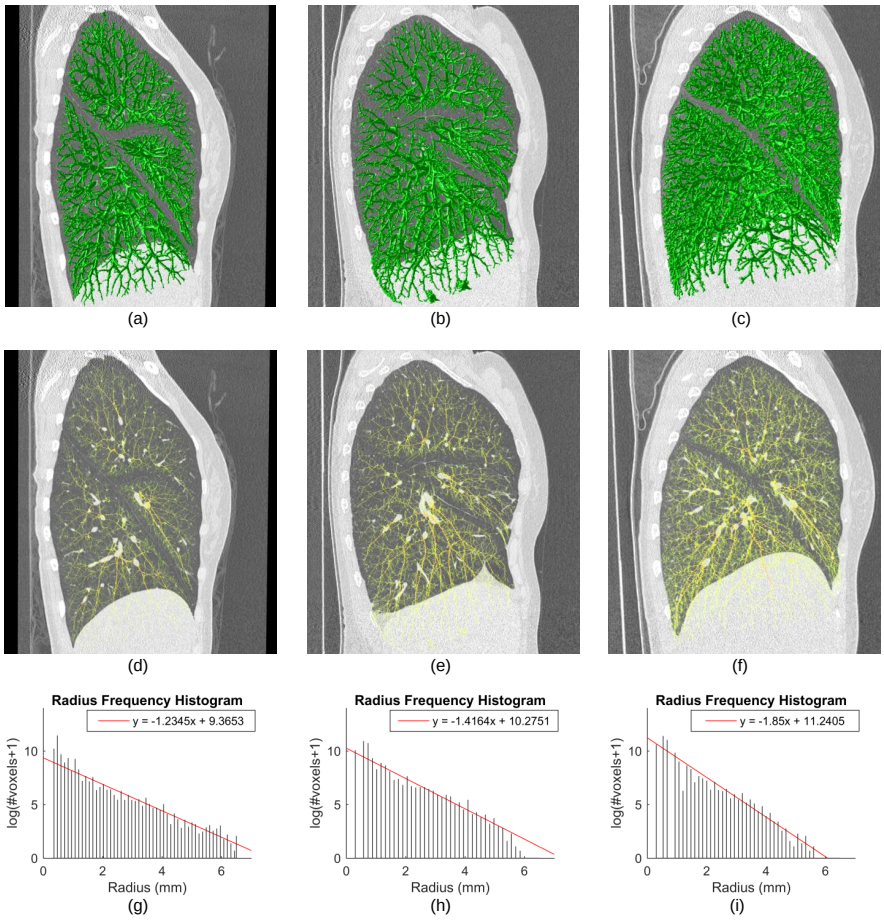

Figure 4.1: Three examples of vascular tree segmentation (a-c), vascular skeleton extraction from the corresponding vascular tree (d-f) and radius frequency histogram analysis of the vascular skeleton trees (g-i). Patient A, B and C had a DLCOc of 46%, 69% and 101.5% predicted, respectively, and lung volumes of 3.81, 6.2 and 4.23 litres, respectively. The loss of vascular tree capacity, i.e., a low intercept β and a flat slope α, is related to impaired gas transfer.

predicted α, β, voxel size and CT-derived lung volume were used as independent variables. A stepwise method was used for selecting significant independent predictors. The same analyses were performed on the subgroup of patients without PH (n=74), i.e. by excluding the three patients with PH confirmed by RHC. All statistical analyses were performed by using SPSS (version 20.0.0, Armonk, NY: IBM Corp.), and a 2-tailed p-value below 0.05 was considered statistically significant.

4.3 Results

The patient characteristics are shown in Table 4.1. In this study, 77 patients (mean age, 49.9 ± 14.2, including 67 females) were investigated, and the time difference between their CT and PFT is 1.19 ± 1.24 days. Among this studied patient group, three patients were confirmed with PH and were classified as pulmonary arterial hypertension (group 1), according to their CO, PVR and PAWP measurements. The average value of α and β were -1.44 ± 0.2 and 10.1 ± 0.62, respectively. Individually, age, α, β and sPAP were moderately but significantly correlated with DLCOc %predicted, as presented in Table 4.2. The age and sPAP were significantly and negatively correlated with DLCOc %predicted. The biomarker α had a significant negative correlation with DLCOc %predicted (R=-0.29, p-value=0.011), which implies that a less negative α (small-vessel pruning or large-vessel dilation) corresponds to a more impaired gas exchange (lower DLCOc %predicted). β had a positive significant correlation with DLCOc %predicted (R=0.32, p-value=0.004), which implies that a lower β (a low capacity of the vascular tree) corresponds to a more impaired gas exchange. The corresponding scatter plots are presented in Figure 4.2.

The results of the multivariable stepwise linear regression analysis for DLCOc %predicted as dependent variable are shown in Table 4.3. The multivariable stepwise regression analysis selected sPAP (coefficient=-0.78, 95%CI=[-1.07, -0.49], p-value<0.001), β (coefficient=8.6, 95%CI=[4.07, 13.12], p-value<0.001) and FEV1 %predicted (coefficient=0.3, 95%CI=[0.12, 0.48], p-value=0.001 as significant and independent predictors of DLCOc %predicted (R=0.71, p-value<0.001). By including β in the model, an additional 10% of variation in gas transfer could be explained (from R=0.56 to R=0.66).

For additional analysis, we evaluated the relationships between imaging biomarkers and pulmonary ventilation i.e. FVC % predicted. As presented in Table 2, the correlation between age, BMI, sPAP, α, β and FVC % predicted was not significant, whereas CT-derived lung volume was significantly correlated with FVC % predicted (R=0.41, p-value<0.001). Furthermore, the correlations between image biomarkers and sPAP were investigated. The correlation between sPAP and BMI (R=0.05, p-value=0.676), α (R=0.08, p-value=0.509), β (R=-0.01, p-value=0.92) and lung volume (R=-0.11, p-value=0.333) were not significant, while age had a significant

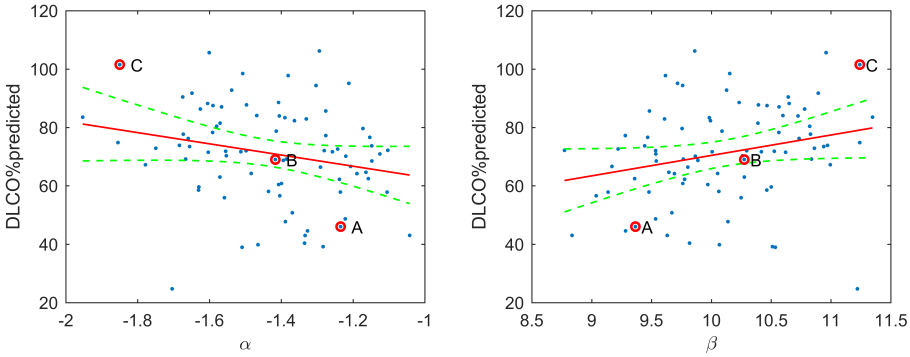

(a) (b)

Figure 4.2: Correlation between imaging biomarkers and lung function (A, B and C are corresponding to patient A, B and C in Figure 1, respectively). (a) Correlation between α and DLCOc % predicted (R=-0.29, p-value=0.011); (b) Correlation between β and DLCOc % predicted (R=0.32, p-value=0.004)

Table 4.2: Correlations, R (p-value), between CT imaging biomarkers and PFTs.

	DLCOc % predicted	FVC % predicted
α	-0.29 (0.011)	-0.14 (0.243)
β	0.32 (0.004)	0.15 (0.187)
sPAP	-0.38 (0.001)	-0.01 (0.909)
BMI	0.19 (0.105)	0.26 (0.023)
Age	-0.29 (0.01)	0.14 (0.23)
Lung Volume	0.18 (0.12)	0.41 (<0.001)

correlation with sPAP (R=0.53, p-value<0.001). In the statistical analyses on the subgroup of patients without PH (n=74), α (R=-0.34, p-value=0.003) and β (R=0.42, p-value<0.001) were significantly correlated with DLCOc %predicted; β was the first selected independent predictor of DLCOc %predicted, followed by sPAP and FEV1 %predicted, in multivariable stepwise regression. The results of the subgroup analyses are shown in the online supplements.

4.4 Discussion

We studied the pulmonary vascular morphology among SSc patients without pulmonary fibrosis. An automatic method was applied to CT images (without contrast medium), for characterizing the pulmonary vasculature by quantifying the vascular system with a radius histogram analysis. To our knowledge, this is the first report on the relationship between pulmonary vascular tree capacity (the number of pulmonary

Table 4.3: Multivariable stepwise linear regression analysis for DLCOc %predicted (n=77).

Parameter	Multivariable regression	
	Regression Coefficient [95% CI]	p-value
Age	-	-
BMI	-	-
sPAP	-0.78 [-1.07, -0.49]	<0.001
FVC %predicted	-	-
FEV1 %predicted	0.3 [0.12, 0.48]	0.001
TLC %predicted	-	-
α	-	-
β	8.6 [4.07, 13.1]	<0.001
Voxel size	-	-
Lung Volume	-	-

capillaries estimated from CT) and gas transfer. Two CT-derived imaging biomarkers were introduced that are significantly correlated with DLCOc % predicted, demonstrating that gas transfer is associated with changes in vascular morphology. This may be useful in understanding the pathophysiology of this subgroup of SSc patients whose gas transfer deteriorates in the course of their disease without detectable pulmonary fibrosis.

Pulmonary vasculature was quantitatively assessed by two measurements, α and β. Biomarker α, the histogram slope, reflects the relative contribution of small vessels compared to large vessels, quantifying pruning of distal vessels and dilatation of the proximal vessels. Biomarker β, the histogram intercept, is estimated by extrapolation to radius 0 which provides an estimate of the vascular tree capacity, without actually detecting pulmonary capillaries. The biomarker α was significantly correlated with biomarker β (R=-0.91, p-value<0.001), implying that the reduction of vascular tree capacity could result in a change in the relative contribution of small vessels compared to large vessels. sPAP, β, FEV1 %predicted were selected by the stepwise method, whereas α, was excluded as it didn't explain additional DLCOc %predicted variation, probably due to the high correlation between α and β. To illustrate the effect of α and β (pruning/dilatation and vascular tree capacity), three patients are discussed in more detail (see Figure 4.1 and 4.2). Patient A with a low DLCOc % predicted obtained a flat slope α and a low intercept β, indicating vessel pruning/dilatation and a loss of vascular tree capacity, as compared to the other patients. This was confirmed by visual inspection of the vascular tree in Figure 4.1. Compared to patient B who had a moderate DLCOc %predicted, α and β, patient C had a higher DLCOc %

predicted, lower α value and higher β value, which implied that a better gas transfer corresponds to a lower vessel pruning/dilatation and higher vascular tree capacity. As the studied patient group consisted of SSc patients without pulmonary fibrosis, CT-derived lung volume was considered to reflect the total lung capacity. Since the voxel size might affect the vascular morphology measurements, voxel size was entered as independent variable in the multivariable linear regression. It proved, however, to be a non-significant factor in predicting gas transfer.

DLCOc % predicted and FEV1 % predicted correlated significantly in our study population (R=0.4, p-value=0.001). In the multivariable linear regression, the FEV1 % predicted was a significant independent predictor of DLCOc % predicted, which implies that pulmonary gas transfer was associated with pulmonary ventilation (air flow). The sPAP had a negative and significant correlation with DLCOc % predicted, and the sPAP was a significant predictor of DLCOc % predicted in the multivariable linear regression, which indicates that pulmonary pressure (blood flow) could affect gas transfer. In the subgroup of patients without PH, the performance of the biomarkers in predicting gas transfer was similar to those of the whole patient group, which implies that excluding or including these three PH patients did not change the validity of the biomarkers.

Several aspects of the correlation between β and DLCOc % predicted as well as the influence of FVC require some clarification. The correlation between DLCOc % predicted and β may be influenced by the position of the patient in both measurements (i.e. the sitting position during gas transfer studies and the supine position during chest CT). Two determinants of DLCO, membrane diffusing capacity (Dm) and capillary blood volume (Vc), have been known to be affected by posture and gravity. A postural change from sitting to the supine position in normal gravity, where some degree of heterogeneity between dependent and nondependent lung region persists, can result in an increase in Vc and not Dm, and an overall increase in DLCO up to 15% [105, 113]. Therefore, it seems plausible that this could have weakened the correlation between β and DLCOc % predicted. Furthermore, since α and β have not been evaluated in normal subjects, values between the "upper and lower limit of normal" of α and β may exist in our study population. This may be another factor that could have led to weakening the correlation between β and DLCOc % predicted. However, the protection of healthy individuals against radiation exposure prevents us from prospectively measuring α and β in CT images from normal controls, and retrospectively collecting negative CT examinations generally lacks confirmation by pulmonary function tests and these CT scans are usually contrast enhanced affecting the vascular morphology analysis.

Currently, studies on quantifying vascular tree morphology with CT imaging also showed promising results for assessing pulmonary vascular pathology associated with other pulmonary diseases. In COPD related studies [12, 60], the pulmonary vessel

morphology was quantified using CT scans without contrast as the percentage of small vessels i.e. vessels with cross-section area less than 5 mm^2 (%CSA<5 mm^2). The quantification had a weak but significant correlation with PFTs [60], and a significant negative correlation with mPAP [12]. Furthermore, smoking-related COPD is characterized by distal pruning of the small vessels which was assessed with the ratio between small vessel volume with CSA<5 mm^2 and total blood vessel volume (BV5/TBV) [62]. In one pulmonary hypertension study [66], pulmonary vascular morphology was quantified with contrast-enhanced chest CT in 24 patients (18 with and 6 without PH). Vascular remodelling characterized by vessel tortuosity and 3D fractal dimensions correlated significantly with RHC measurements. Furthermore, in chronic thromboembolic pulmonary hypertension (CTEPH), the disease was quantified as pulmonary morphologic changes with CT scans [65], including pruning of the distal vessel and dilation of the proximal vessels which were measured with the ratio BV5/TBV and the ratio BV>10/TBV (where BV>10 is the blood volume for all vessels with a CSA>10 mm^2), respectively. These biomarkers differed significantly between CTEPH patients and control individuals, and they correlated with RHC measures. In this study quantification on portions of pulmonary vascular system based on CSA or quantification of the pulmonary vascular fractal dimension was performed. In our study, however, we considered the pulmonary vessels as a continuous system, by quantifying vascular changes including all vessel radii by histogram analysis, instead of analysing only parts of the vascular tree. This yielded two biomarkers, α and β, that characterized the vascular tree in a more global approach and showing an association with gas transfer.

There are some limitations in our analysis. The automatic method used in the present study could not distinguish arteries from veins. As vascular changes may differ between arteries and veins, improved correlation may be expected with arteries evaluated separately from veins. However, even without this distinction, we already found a significant association with gas transfer. Also, we assessed both lungs together for each patient. More specific analysis of separate lungs or lung lobes may provide a more localized assessment of vascular changes. All patients in this study were scanned by the same scanner, thus, when adopting the automatic method to other CT scanners, the parameters for vessel extraction might need to be adjusted. The studied group only included SSc patients without a control group. Data on normal vasculature morphology of healthy people would enhance our understanding. Nevertheless, our method was still able to detect variances in the pulmonary vasculature. Due to a lack of pathology specimens in these SSc patients, validation of the imaging measurements against pathology was not possible. In the future, we aim to prospectively follow-up changes in the pulmonary vascular morphology in these patients over time, and evaluate if these subtle changes precede functional changes in pulmonary testing.

Studying the morphological changes of pulmonary vasculature in the patients with PH related diseases, such as chronic thromboembolic pulmonary hypertension, is also an interesting point of our future work, as the metric of morphological changes could help to predict an early development or monitor effects of treatment.

4.5 Conclusion

In conclusion, we characterized the pulmonary vasculature by two CT-derived imaging biomarkers from vascular radius analysis. These two imaging biomarkers, indicating small-vessel-pruning/large-vessel-dilation and loss of vascular tree's capacity, are associated with decreased gas transfer in the studied SSc patient group. The method may help understand the relationship between pulmonary vascular changes in SSc and lung function, in the absence of detectable fibrosis.

Supplementary

Segmentation methods

Three atlases that were labelled manually by pulmonary experts with Pulmo CMS software [114] were taken as moving image, and patient images were taken as fixed images. The torso masks were generated automatically using Pulmo-CMS, and were used to eliminate the influence of external objects on image registration quality. The registrations included an affine registration to tackle differences in the body positioning and a B-spline deformable registration to tackle anatomical differences in lung shape. The B-spline transformation model was subsequently used to transform the lung mask from the moving to the fixed image. After these procedures, three candidate lung masks corresponding to three atlases were fused by majority voting.

For lung vessels segmentation, a number of methods have been proposed in the literature. According to the challenge "Vessel Segmentation in the Lung 2012" (VESSEL12) [41], vesselness filters based on analysing the eigenvalues of the Hessian matrix were most successful. However, due to the low response at vessel boundaries and bifurcations, and the non-uniform response between vessels of different radii, extracting lung vessels by simply thresholding the vesselness is not sufficiently accurate for pulmonary vessel radius analysis. In this study, we therefore used a graph-cuts based method for the ultimate lung vessel segmentation, with a specifically designed cost function. The details on this vessel segmentation method have been described previously [111]. All image processing experiments were performed on a local PC with 24 GB RAM memory, Intel Xeon W3520 CPU with 4 cores, with 64-bit Windows 7 Professional OS.

Table A1. Evaluation of the multi-atlas based lung volume segmentation method.

ID	Dice	HausdorffD	AveSurfaceD	StdSurfaceD
1	0.987	23.431	0.355	0.895
2	0.986	23.791	0.431	1.077
3	0.986	27.677	0.466	1.210
4	0.960	39.064	1.468	2.521
5	0.986	19.672	0.515	0.986
6	0.989	24.062	0.423	1.015
7	0.984	23.622	0.490	1.061
8	0.982	23.087	0.593	1.410
9	0.988	21.633	0.497	1.056
10	0.987	32.265	0.508	1.150
11	0.987	21.749	0.435	0.929
12	0.977	30.887	0.905	2.135
13	0.977	26.926	0.818	1.982
14	0.989	22.226	0.403	0.894
15	0.980	24.000	0.643	1.259
16	0.987	24.352	0.394	1.132
17	0.988	20.518	0.455	1.166
18	0.987	23.043	0.442	1.092
19	0.986	27.586	0.458	1.075
20	0.987	23.622	0.491	0.986
Average	0.984	25.161	0.559	1.252
The unit of distance measurements is mm				

Evaluation of lung segmentation

For the evaluation of our automatic lung segmentation method, 20 patients, who were randomly selected from SSc patients group, with manually labelled lung volume were used. Volume overlap similarity (Dice), maximum surface distance (Hausdorff distance HausdorffD), average surface distance (AveSurfaceD) and standard deviation of the surface distance (StdSurfaceD) were used for evaluating the multi-atlas-based lung segmentation method. As shown in Table A1, the average Dice of 20 patients was 0.984, the average Hausdorff distance was 25.161 mm, average AveSurfaceD was 0.559 mm and average StdSurfaceD was 1.252. From the Dice, AveSurfaceD and StdSurfaceD, it can be concluded that the segmentation method generally performed quite well. For the large Hausdorff distance, we visually checked the segmentation results and the maximum surface distance occurred at the border and corner of the lung region. Since vessels are rarely located at the lung boundary, these errors are not relevant and the ultimate segmentation results were reliable.

Evaluation of lung vessel segmentation

The public data-set of 20 CT scans from the VESSEL12 challenge was used for evaluating the vascular tree extraction method. The extracted lung vessels were submitted to the challenge organizer and evaluations were sent back. Our method obtained an area under the ROC curve (Az) of 0.975, which is a competitive performance on VESSEL12, especially among the binary submissions. The method performed well for the small vessels, medium vessels and large vessels, but for separating the airway wall, dense lesion and bronchi from the lung vessels, performance was less successful.

Results of subgroup (n=74) without PH

Among the patient group in this study, three patients out of 77 were confirmed in Pulmonary Hypertension (PH). To understand the biomarkers' effect in predicting gas transfer, the same statistical analyses were carried out in the subgroup (n=74) by excluding three PH patients. The results of Spearman's correlation analysis are presented in Table A3, where α (R=-0.34, p-value=0.003) and β (R=-0.42, p-value<0.001) were significantly correlated with DLCOc %predicted. From the results of multivariable stepwise regression, as demonstrated in Table A4, the biomarkers β (coefficient=8.33, 95% CI=[3.72, 12.9], p-value=0.001), was the firstly selected significant independent variables of DLCOc %predicted (R=0.65, p-value<0.001). Thus, in comparison with the statistical results of whole patient group, the performance of biomarkers in predicting gas transfer was the same, which implies that excluding or including three PH patients does not change the validity of biomarkers.

Discussion

For the automatic image processing methods used in this study, the atlas-based lung segmentation method was evaluated using 20 patients of in-house data against manually segmented lung fields labelled by experts. The results (Table A1) showed that the average Dice index was 0.984 and the average mean-surface-distance was 0.55 mm, which implies that our lung segmentation method is reliable. The lung segmentation method may be improved further by including more atlases. The graph-cuts based method, which was applied for vascular tree extraction, was evaluated with the public data set and obtained accurate results, especially among the binary vessel extraction methods. The graph-cuts method performed quite well for vessel segmentation for the small vessels, medium vessels and large vessels, but it failed to separate touching airway walls and vessels, which was caused mainly by similar intensity and adjacency between airway walls and vessels. Taking CT intensity into the cost function of the graph-cuts method made the detection of vascular boundaries and bifurcations more accurate, but the noise in CT produces a rough surface. To address this shortcoming, the subdivision method [115], which is a tube surface

Table A2. Characteristics of subgroup patients

Number of subjects	74
Female n [%]	65 [87.8]
Age (year)	49.2 ± 13.9
BMI (kg/m^2)	24.6 ± 5.34
sPAP (mmHg)	25.3 ± 5.95
MRSS	3.34 ± 4.36
Type of SSc n [%]	
DcSSc	8 [10.8]
LcSSc	48 [64.9]
LSSc	18 [24.3]
Autoantibodies, n [%]	
ANA	71 [95.9]
Anti-Scl-70 #	4 [5.5]
Anticentromere *	51 [68.9]
RNA polymerase III	1 [1.4]
Pulmonary function (% predicted**)**	
DLCO	71.9 ± 15.3
FVC	108 ± 16.6
FEV_1	100 ± 14.9
TLC	96.3 ± 11.7
CT-derived measurements	
α	-1.44 ± 0.2
β	10.1 ± 0.61
Lung Volume (L)	4.73 ± 1.23

1 patient with doubtful Anti-Scl-70. * 1 patient with missing data.

Table A3. Correlations, R (p-value) between CT imaging biomarkers and PFTs.

	DLCO % predicted	FVC % predicted
α	-0.34 (0.003)	-0.17 (0.154)
β	0.42 (<0.001)	0.24 (0.041)
sPAP	-0.30 (0.009)	0.11 (0.372)
BMI	0.22 (0.063)	0.29 (0.013)
Age	-0.22 (0.063)	0.24 (0.038)
Lung Volume	0.18 (0.133)	0.42 (<0.001)

Table A4. Multivariable stepwise linear regression analysis for DLCOc %predicted (n=74).

	Multivariable regression	
Parameter	Regression Coefficient [95% CI]	p-value
Age	-	-
BMI	-	-
sPAP	-0.99 [-1.46, -0.53]	<0.001
FVC %predicted	-	-
FEV1 %predicted	0.33 [0.14, 0.52]	0.001
TLC %predicted	-	-
α	-	-
β	8.33 [3.72, 12.9]	0.001
Voxel size	-	-
Lung Volume	-	-

fitting algorithms with centreline as reference, might provide better surfaces and more accurate radius estimation. The skeletonisation method, which was carried out by a symmetric distance transform, would then provide accurate centres of the skeleton and estimate the radius reliably. However, with the current rough surface, some side branches may still remain, despite the removal of easily-distinguished side branches by the skeletonisation method [86]. Therefore, centreline tracing methods may be beneficial for removing these side branches.